Eur J Nucl Med Mol Imaging (2010) 37:934–941
DOI 10.1007/s00259-009-1314-7

ORIGINAL ARTICLE

In vivo detection of prion amyloid plaques using [^{11}C]BF-227 PET

Nobuyuki Okamura · Yusei Shiga · Shozo Furumoto · Manabu Tashiro · Yoshio Tsuboi · Katsutoshi Furukawa · Kazuhiko Yanai · Ren Iwata · Hiroyuki Arai · Yukitsuka Kudo · Yasuhito Itoyama · Katsumi Doh-ura

Received: 7 August 2009 / Accepted: 21 October 2009 / Published online: 17 December 2009

Abstract

Purpose In vivo detection of pathological prion protein (PrP) in the brain is potentially useful for the diagnosis of transmissible spongiform encephalopathies (TSEs). However, there are no non-invasive ante-mortem means for detection of pathological PrP deposition in the brain. The purpose of this study is to evaluate the amyloid imaging tracer BF-227 with positron emission tomography (PET) for the non-invasive detection of PrP amyloid in the brain.

Methods The binding ability of BF-227 to PrP amyloid was investigated using autoradiography and fluorescence microscopy. Five patients with TSEs, including three patients with Gerstmann-Sträussler-Scheinker disease (GSS) and two patients with sporadic Creutzfeldt-Jakob disease (CJD), underwent [^{11}C]BF-227 PET scans. Results were compared with data from 10 normal controls and 17 patients with Alzheimer's disease (AD). The regional to pons standardized uptake value ratio was calculated as an index of BF-227 retention.

Results Binding of BF-227 to PrP plaques was confirmed using brain samples from autopsy-confirmed GSS cases. In clinical PET study, significantly higher retention of BF-227 was detected in the cerebellum, thalamus and lateral temporal cortex of GSS patients compared to that in the corresponding tissues of normal controls. GSS patients also showed higher retention of BF-227 in the cerebellum, thalamus and medial temporal cortex compared to AD patients. In contrast, the two CJD patients showed no obvious retention of BF-227 in the brain.

Conclusion Although [^{11}C]BF-227 is a non-specific imaging marker of cerebral amyloidosis, it is useful for in vivo detection of PrP plaques in the human brain in GSS, based on the regional distribution of the tracer. PET amyloid imaging might provide a means for both early diagnosis and non-invasive disease monitoring of certain forms of TSEs.

N. Okamura · S. Furumoto · K. Yanai
Department of Pharmacology,
Tohoku University School of Medicine,
Sendai, Japan

Y. Shiga · Y. Itoyama
Department of Neurology,
Tohoku University School of Medicine,
Sendai, Japan

S. Furumoto · R. Iwata
Division of Radiopharmaceutical Chemistry,
Cyclotron and Radioisotope Center, Tohoku University,
Sendai, Japan

M. Tashiro
Division of Cyclotron Nuclear Medicine,
Cyclotron and Radioisotope Center, Tohoku University,
Sendai, Japan

Y. Tsuboi
Department of Neurology,
Fukuoka University School of Medicine,
Fukuoka, Japan

K. Furukawa · H. Arai
Department of Geriatrics and Gerontology,
Division of Brain Sciences, Institute of Development,
Aging, and Cancer, Tohoku University,
Sendai, Japan

Y. Kudo
Innovation of New Biomedical Engineering Center,
Tohoku University,
Sendai, Japan

K. Doh-ura (✉)
Department of Prion Research,
Tohoku University School of Medicine,
2-1 Seiryo-machi, Aoba-ku, Sendai 980-8575, Japan
e-mail: doh-ura@mail.tains.tohoku.ac.jp

Keywords Prion · PET · Amyloid · Creutzfeldt-Jakob disease

Introduction

Transmissible spongiform encephalopathies (TSEs), also known as prion diseases, are a group of fatal neurodegenerative disorders, including Creutzfeldt-Jakob disease (CJD), Gerstmann-Sträussler-Scheinker disease (GSS) and kuru [1–3]. TSEs are characterized by progressive deposition of abnormal prion protein (PrP) in the brain. CJD is the most common type of human TSE and is classified into sporadic, genetic and infectious forms according to the aetiology of illness. GSS is a familial neurodegenerative disorder associated with mutations of the PrP gene and is clinically recognized by cerebellar ataxia combined with postural abnormalities and cognitive decline [1–3]. Two major types of abnormal PrP deposition, synaptic and plaque types, have been described in the brain of people with TSEs [1]. The synaptic type of PrP deposition, which does not have tinctorial properties of amyloid in tissue sections, is most commonly observed in sporadic CJD, whereas the plaque type, which frequently forms congophilic amyloid plaques, is a hallmark of such TSEs as GSS, variant CJD (vCJD) and iatrogenic dura CJD with plaques [1, 4]. Abnormal PrP deposition in the brain is suggested to start before the occurrence of clinical symptoms [5–7]. Thus, preclinical diagnosis and, when available, early disease-specific therapeutic interventions, can be beneficial for people predisposed to or affected by TSEs.

Several positron emission tomography (PET) imaging agents have been recently developed and used for in vivo detection of brain amyloid-β (Aβ) plaques in patients with Alzheimer's disease (AD) [8–12]. Most of these β-sheet binding agents show high binding affinity to PrP amyloid because PrP aggregates in TSEs form β-pleated sheet structures and share a common secondary structure with Aβ deposits in AD brains [13–16]. Therefore, these agents would be useful for the in vivo detection of PrP amyloid in the brain. Two clinical PET studies were performed using [^{18}F]FDDNP and/or [^{11}C]PIB in sporadic and familial CJD patients [17, 18]. The results indicated moderate retention of FDDNP and no obvious retention of PIB in the brain [17, 18]. Therefore, agents that can sensitively detect abnormal PrP deposits should be further explored for the diagnosis of TSEs. We have demonstrated in vitro and in vivo binding of benzoxazole derivatives to both Aβ and PrP amyloids [19, 20]. One of these derivatives, BF-227, was used for a clinical PET study where it successfully visualized amyloid deposits in the brain of AD patients in vivo [12, 21]. Therefore, [^{11}C]BF-227 appears to be a promising candidate for PET imaging of PrP deposits. The purpose of this study was to evaluate the clinical utility of [^{11}C]BF-227 PET for the non-invasive detection of abnormal PrP deposits in patients with TSEs.

Methods

Preparation of compounds

BF-227 and its 2-tosyloxyethoxy and *N*-desmethylated derivatives were custom synthesized by Tanabe R&D Service Co. (Osaka, Japan). [^{18}F]BF-227 was synthesized for autoradiography of brain sections, as described previously [22]. For the clinical studies, [^{11}C]BF-227 was synthesized as described previously [12]. Radiochemical yields were greater than 50% based on [^{11}C]methyl triflate, and specific radioactivities were 119–138 GBq/μmol at the end of synthesis. Radiochemical purities were greater than 95%.

Histopathological staining and in vitro autoradiography

Autopsy-diagnosed brain samples from two GSS cases with PrP plaque deposition and two sporadic CJD cases with synaptic PrP deposition were provided by Dr. Toru Iwaki of the Department of Neuropathology, Kyushu University, Japan. The brain sample from an 81-year-old man with autopsy-confirmed physiological aging was obtained from Tohoku University Hospital. The two GSS cases had a proline-to-leucine mutation at codon 102 and methionine homozygosity at codon 129 of the PrP gene, and the two sporadic CJD cases had no mutations and methionine homozygosity at codon 129; they showed type 1 abnormal PrP in immunoblotting of the brain tissues. All of the brain samples were treated with 98% formic acid for 1 h before paraffin embedding to eliminate prion infectivity. Sections from paraffin-embedded blocks of the cerebellum or frontal cortex were then dewaxed in xylene and ethanol. For staining with BF-227, tissue sections were immersed in 100 μM BF-227 solution containing 50% ethanol for 10 min. They were then dipped briefly into water and rinsed in phosphate-buffered saline for 10 min before coverslipping with FluorSave Reagent (Calbiochem, La Jolla, CA, USA). Subsequently, they were examined using an Eclipse E800 microscope (Nikon, Tokyo, Japan) equipped with a V-2A filter set (excitation, 380–420 nm; dichroic mirror, 430 nm; Longpass filter, 450 nm). For autoradiography, the section was incubated with 1.0 MBq/ml of [^{18}F]BF-227 at room temperature for 10 min and then washed briefly with water and 50% ethanol. After drying, the labelled section was exposed to a BAS-III imaging plate (Fuji Film, Tokyo, Japan) overnight. Autoradiographic images were obtained using a BAS-5000 phosphor imaging instrument (Fuji Film, Tokyo, Japan). Neighbouring sec-

tions were immunostained using 3F4 anti-PrP monoclonal antibody (Covance, Princeton, NJ, USA) as described previously [13, 20].

Subjects and patients in the clinical PET study

Five TSE patients, including two sporadic CJD patients [63-year-old woman (CJD1) and 58-year-old man (CJD2)] and three GSS patients [69-year-old woman (GSS1), 61-year-old man (GSS2) and 30-year-old woman (GSS3)], underwent PET scans with [^{11}C]BF-227 (Table 1). For comparison, [^{11}C]BF-227 PET studies were also performed in 17 AD patients [mean age ± standard deviation (SD)= 72.6±6.7; mean Mini-Mental State Examination score ± SD=19.8±4.0] and 10 aged normal controls (mean age ± SD=67.2±2.5). Some of these AD and normal subjects were included in our previous report [12].

CJD1's health was unremarkable until the manifestation of depressive symptoms at the age of 62 years. The patient then developed subacutely progressive dementia, motor disturbances and myoclonus. CJD2 showed subacutely progressive dementia and gait disturbance and then developed psychotic symptoms, dysarthria and myoclonus. Both CJD patients had no mutations and showed methionine homozygosity at codon 129 of the PrP gene. PET studies in CJD1 and CJD2 were performed when they reached grade 4 of the modified Rankin scale at 3 and 4 months after onset of symptoms, respectively. Both patients showed periodic synchronous discharges in electroencephalograms and hyperintensity in the caudate, putamen and cerebral cortex on diffusion-weighted magnetic resonance (MR) images. Diagnosis of probable CJD was made according to the WHO criteria [23].

Each GSS patient was from a different pedigree and had a family history of the same disease, carrying a proline-to-leucine mutation at codon 102 and methionine homozygosity at codon 129 of the PrP gene. GSS1 and GSS2, having a 9- and 20-month clinical duration from the onset, respectively, showed signs of moderate cerebellar ataxia, such as gait disturbance and slurred speech; however, they could walk unassisted and had slight or no cognitive impairment. GSS1 and GSS2 scored 22 and 26 points, respectively, on the Mini-Mental State Examination. GSS3, having a 27-month clinical duration, showed severe gait disturbance and slurred speech and was unable to walk unassisted; however, she had no cognitive impairment (30 points on the Mini-Mental State Examination) at the time of this study.

AD diagnosis was made according to the National Institute of Neurological and Communicative Diseases and Stroke-Alzheimer's Disease and Related Disorders Association (NINCDS-ADRDA) criteria [24]. CJD, GSS and AD patients were recruited from Miyagi National Hospital, Fukuoka University Hospital, Kagoshima University Hospital and Tohoku University Hospital. Normal controls were recruited from volunteers with no cognitive impairment or cerebrovascular lesions on MR images and who were not taking any centrally acting medications. No significant difference in age distribution was apparent between the groups. This study was approved by the Ethics Committee on clinical investigations of Tohoku University School of Medicine and performed in accordance with the Declaration of Helsinki. Written informed consent was obtained after complete description of the study to the patients and subjects.

Image acquisition protocols

PET scans were performed using a SET-2400W (Shimadzu Inc., Kyoto, Japan). After intravenous injection of 211–366 MBq (5.7–9.9 mCi) of [^{11}C]BF-227, dynamic PET images were obtained for 60 min with the subjects' eyes closed. Arterial blood sampling in the TSE patients was not

Table 1 Regional to pons standardized uptake value ratio (SUVRp) values in aged normal controls (Control), Alzheimer's disease patients (AD), Creutzfeldt-Jakob disease patients (CJD) and Gerstmann-Sträussler-Scheinker disease patients (GSS)

	Control (n=10) Mean ± SD	AD (n=17) Mean ± SD	CJD1	CJD2	GSS (n=3) Mean ± SD	GSS1	GSS2	GSS3
Frontal	0.60±0.03	0.64±0.04	0.57	0.61	0.67±0.08	0.74	0.69	0.57
Lateral temporal	0.59±0.03	0.69±0.04*	0.63	0.62	0.67±0.05*	0.71	0.68	0.61
Parietal	0.62±0.02	0.69±0.04*	0.62	0.62	0.67±0.06	0.72	0.68	0.61
Occipital	0.62±0.04	0.65±0.05	0.62	0.69	0.67±0.07	0.74	0.67	0.60
Medial temporal	0.64±0.04	0.62±0.03	0.57	0.65	0.67±0.02**	0.66	0.70	0.67
Striatum	0.71±0.04	0.75±0.04*	0.69	0.72	0.76±0.04	0.80	0.77	0.72
Thalamus	1.00±0.04	1.01±0.04	0.97	1.04	1.08±0.00*, **	1.08	1.07	1.08
Cerebellum	0.58±0.01	0.57±0.02	0.58	0.59	0.62±0.01*, **	0.61	0.63	0.61

*p<0.05 compared to aged normal group

**p < 0.05 compared to AD group

performed because the Committee on Clinical Investigation at Tohoku University School of Medicine did not approve blood sampling during the PET scan, from the standpoint of infection risk management. T_1-weighted MR images were obtained using a Signa 1.5-T machine (General Electric Inc., Milwaukee, WI, USA).

Image analysis

Standardized uptake value (SUV) images of [^{11}C]BF-227 were obtained by normalizing tissue concentration by injected dose and body weight. Average summations of SUV images were created from early frames (0–30 min post-injection) and late frames (40–60 min post-injection) of dynamic PET images. Early frame images were created for co-registration with individual MR images, and late frame images were used for calculation of SUV. Individual MR images were anatomically co-registered with the early frame PET images using statistical parametric mapping software (SPM2, Welcome Department of Imaging Neuroscience, London, UK) [25]. Spatial normalization was performed using an MR T_1 template of SPM2 to transfer PET images into a standard stereotactic space. Regions of interest (ROIs) were placed on a spatially normalized MR image, as described previously [12]. ROI information was then copied onto delayed PET SUV images, and regional SUV images at 40–60 min post-injection were sampled using Dr.View/LINUX software (AJS, Tokyo, Japan). Deposition of PrP plaques is reportedly frequent in the cerebellum but scarce in the pons of GSS brain [26]. Furthermore, BF-227 retention in the pons does not differ between AD patients and normal controls. Therefore, we used the pons as a reference region and calculated the regional to pons SUV ratio (SUVRp) as an index of BF-227 retention.

Statistical analysis

For statistical comparison in each group, we applied one-way analysis of variance, followed by the Bonferroni-Dunn post hoc test. Statistical comparison of age distribution was performed using the Kruskal-Wallis test, followed by Dunn's multiple comparison test. Statistical significance for each analysis was defined as $p<0.05$.

Results

Autoradiography examination indicated binding of a tracer dose of BF-227 to PrP plaque deposits. BF-227 retention was present in brain sections from GSS cases with PrP plaque deposition but not from normal control cases and sporadic CJD cases with synaptic PrP deposition (Fig. 1a–c). The regional distribution of [^{18}F]BF-227 in the autoradiograms co-localized with the immunostained PrP plaques in the cerebellar cortex of GSS cases (Fig. 1d–e). BF-227 binding to PrP plaques was additionally examined using a microscope, because BF-227 is a fluorescent compound. Core regions of the PrP plaques were intensely stained with BF-227 (Fig. 2, arrows), indicating that BF-227 preferentially binds to the fibril-rich core of PrP amyloid plaques.

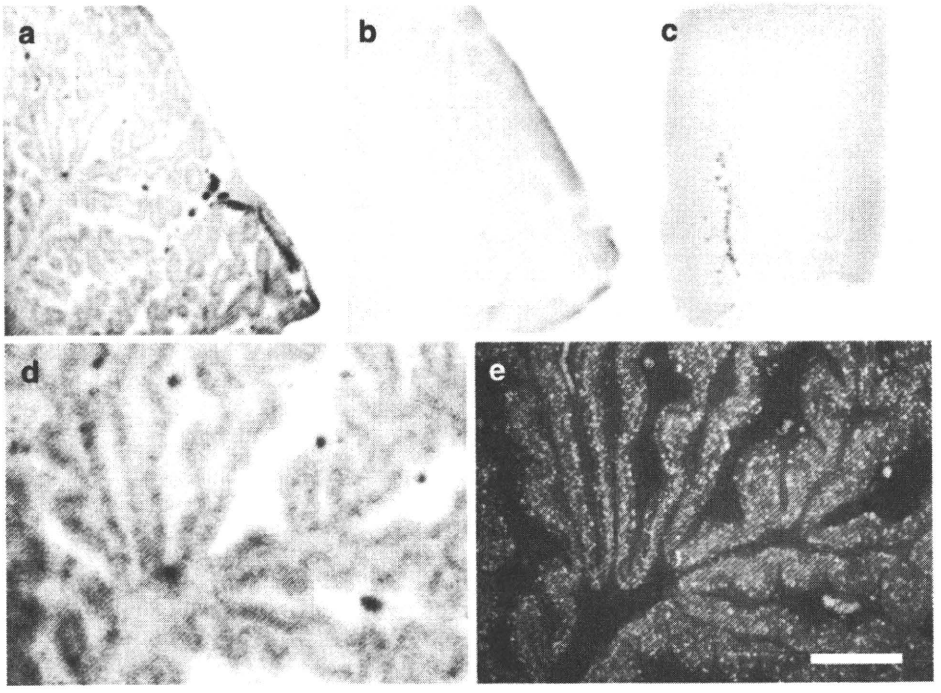

Fig. 1 [^{18}F]BF-227 autoradiograms of a cerebellar section from a Gerstmann-Sträussler-Scheinker (GSS) case (**a**), a cerebellar section from a physiological aging case (**b**) and a frontal cortex section from a sporadic Creutzfeldt-Jakob disease (CJD) case (**c**) are shown, together with a magnified view of **a** (**d**) and prion protein (PrP) immunostaining of the same field as **d** (**e**). BF-227 retention was present in the brain section from a GSS case with PrP plaque deposition, but not from a normal control case and sporadic CJD case with synaptic PrP deposition. *Bar*=200 μm

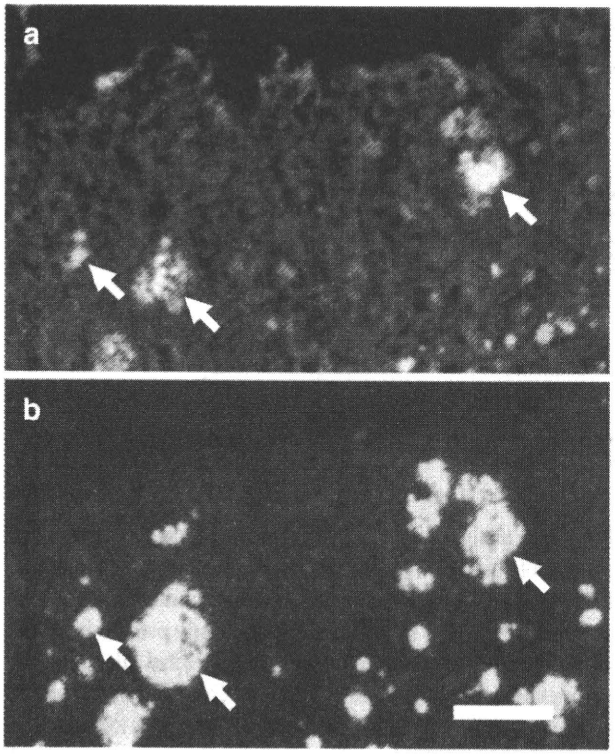

Fig. 2 Microscopic images of BF-227 staining (**a**) and PrP immunostaining (**b**) of the cerebellar cortex of a GSS case. *Arrows* indicate PrP amyloid plaques. The core regions of PrP plaques were intensely stained with BF-227. *Bar*=50 μm

Figure 3 shows the average summations of SUVRp images in an aged normal subject (64-year-old man), a sporadic CJD patient (CJD1, 63-year-old woman), a GSS patient (GSS2, 61-year-old man) and an AD patient (62-year-old woman). As reported previously, non-specific retention of [^{11}C]BF-227 was observed in the brain stem and white matter of all subjects [12]. The GSS patient showed obvious retention of [^{11}C]BF-227 in the cerebellum, and lateral and medial temporal cortices. The three GSS patients showed significantly higher SUVRp in the lateral temporal cortex, thalamus and cerebellum (Table 1, Fig. 4) when compared to aged normal controls. Furthermore, when compared to the AD group, the GSS group showed significant elevation of SUVRp in the medial temporal cortex, thalamus and cerebellum. Although two GSS patients (GSS1 and GSS2) showed retention of BF-227 in most brain regions, the youngest GSS patient (GSS3) showed BF-227 retention only in the cerebellum, thalamus and medial temporal cortex, but not in the neocortex (Table 1, Fig. 4). Furthermore, two sporadic CJD patients showed no obvious BF-227 retention in any of the brain regions examined (Table 1, Fig. 4). As previously described [12, 21], AD patients showed [^{11}C]BF-227 retention in the neocortex; however, the cerebellum and medial temporal cortex were relatively spared (Table 1).

Autopsy examination of the brain of one GSS patient (GSS1) confirmed both the presence of abundant PrP amyloid plaques in the neocortex, cerebellum, basal ganglia, thalamus, entorhinal cortex and hippocampus and the absence of Aβ amyloid plaques or other structures of misfolded protein deposition such as Lewy bodies and neurofibrillary tangles. When compared to controls, the highest SUVRp percentage difference was found in the neocortex, especially in the frontal cortex (22%), followed by the striatum (12%), thalamus (9%), cerebellum (6%) and medial temporal cortex (3%) in this case. This finding was consistent with the autopsy result showing higher density of PrP amyloid plaques in the neocortex and basal ganglia than in the cerebellum, thalamus and hippocampus. Details of clinicopathological features of this case will be published elsewhere.

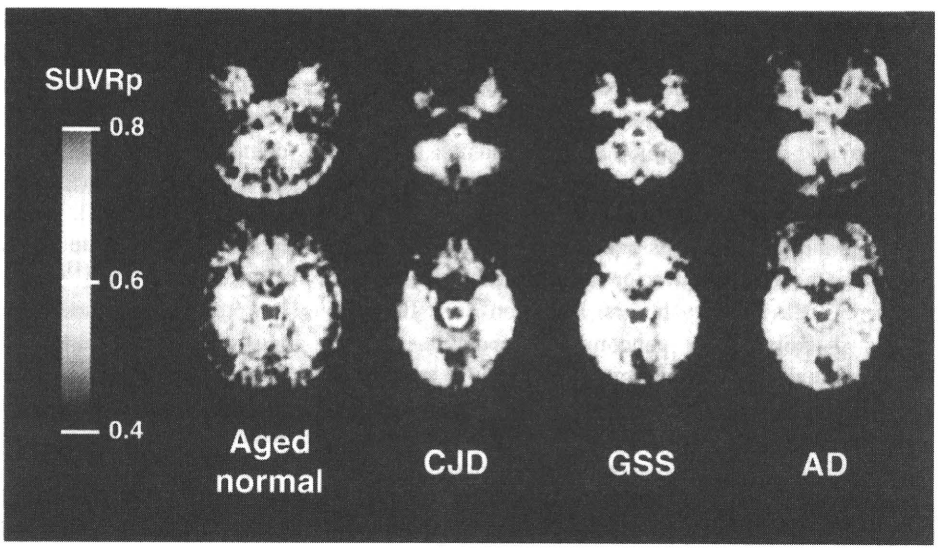

Fig. 3 Mean regional to pons standardized uptake value ratio (SUVRp) images between 40 and 60 min post-injection of [^{11}C]BF-227 in an aged normal subject (64-year-old man), a sporadic CJD patient (CJD1, 63-year-old woman), a GSS patient (GSS2, 61-year-old man) and an AD patient (62-year-old woman). Compared to the aged normal subject and CJD patient, the GSS patient showed obvious [^{11}C]BF-227 retention in the cerebellum and temporal cortex. The AD patient also showed obvious [^{11}C]BF-227 retention in the temporal cortex; however, the cerebellum was relatively spared

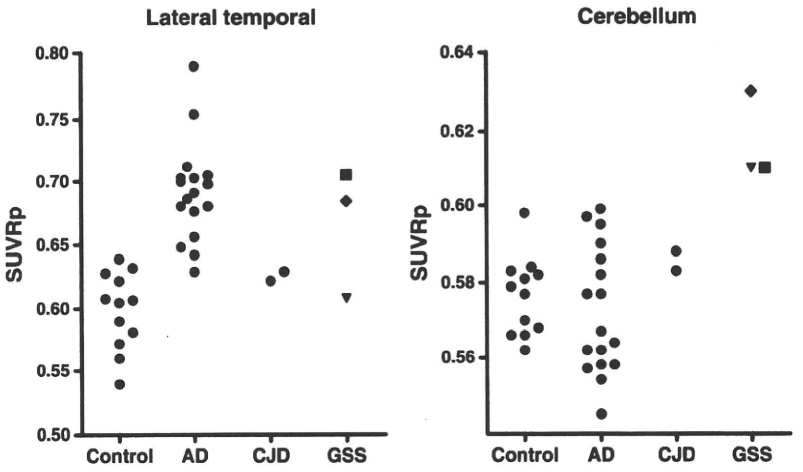

Fig. 4 SUVRp distribution in aged normal controls (*Control*), AD patients (*AD*), CJD patients (*CJD*) and GSS patients (*GSS*). GSS patients showed higher SUVRp values in the lateral temporal cortex and cerebellum. *Filled square* GSS1, *filled diamond* GSS2, *filled inverted triangle* GSS3

Discussion

This is the first study to demonstrate non-invasive detection of PrP amyloid plaques in GSS patients. GSS is neuropathologically characterized by deposits of multicentric amyloid plaques, which are especially abundant in the cerebellum, cerebral cortex and basal ganglia [3]. The present study demonstrated binding of BF-227 to PrP amyloid plaques in GSS brain sections. [^{11}C]BF-227 retention was observed in cortical and subcortical brain regions of GSS patients known for the high density of PrP plaques. Based on these findings, [^{11}C]BF-227 represents a promising candidate PET probe for the non-invasive detection of PrP amyloid plaques in the brain. However, the possibility that neocortical elevation of SUVRp in GSS patients might be caused by concomitant Aβ amyloid deposits or other misfolded protein deposits also should be considered, given that the two GSS patients showing prominent neocortical retention of [^{11}C]BF-227 were relatively older than the GSS patient showing no neocortical retention of BF-227. Although one positive GSS patient (GSS2) is still alive and was not examined neuropathologically, another positive case (GSS1) showed a high level of PrP amyloid deposits but no obvious deposits of Aβ amyloid or other misfolded proteins at autopsy. Furthermore, significant elevation of SUVRp was detected in the cerebellum, thalamus and hippocampus of all GSS cases. These brain regions are known to contain lower densities of Aβ plaques or other misfolded protein structures such as Lewy bodies. Based on these findings, it seems unlikely that concomitant deposition of Aβ amyloid or other misfolded proteins contributes to the high [^{11}C]BF-227 retention in GSS patients.

There is an increasing demand for in vivo detection of abnormal PrP deposition in the brain for the diagnosis of TSEs that might translate in early therapeutic intervention. Although GSS and other familial forms of TSEs can be diagnosed with PrP gene analysis using peripheral blood cells, it has been impossible to non-invasively measure the amount of abnormal PrP deposition in the brain. In a fashion similar to GSS, PrP amyloid deposition in the brain is commonly present in vCJD in which PrP amyloid plaques, called florid plaques, are pathognomonic [27]. Thus, [^{11}C]BF-227 PET might be a sensitive probe for the detection of PrP amyloid plaque deposition in vCJD as well as GSS, allowing longitudinal monitoring of PrP amyloid plaque deposition in the brain. Ante-mortem diagnosis of vCJD relies on the detection of abnormal PrP deposition in tonsil biopsy samples [28]. However, functional imaging using PET has an advantage over surgical biopsy tests in terms of both a non-invasive and an infection risk management point of view.

GSS is a rare form of TSE occurring in only about 3% of TSE cases in Japan. However, GSS is probably one of the TSEs most likely to benefit from early therapeutic interventions because the disease can be confirmed earlier using PrP gene analysis and progression occurs much more slowly than that in sporadic CJD, which comprises the majority of TSE cases. Recently, compounds such as pentosan polysulphate and doxycycline have been clinically used for experimental treatments for TSEs to prevent deposition of abnormal PrP in the brain, because these compounds slowed the disease progression in animal disease models when administered in an earlier stage of the disease [29–33]. Reliable surrogate markers are also required to evaluate the efficacy of these experimental interventions, and [^{11}C]BF-227 PET might be one of the best candidates to assess PrP amyloid deposition in GSS. However, it remains to be elucidated if PrP amyloid levels are a particularly relevant marker of therapeutic efficacy.

A previous PET study demonstrated moderate FDDNP retention and no remarkable PIB retention in the brain of two familial CJD patients with an octapeptide repeat insertion mutation [17]. A recent PET study has additionally demonstrated no PIB retention in two autopsy-confirmed sporadic

CJD patients [18]. In contrast with these studies, the present study successfully demonstrated prominent [^{11}C]BF-227 retention in the brain of GSS patients. Differences between the previous and present findings might mainly reside in the amount and type of PrP amyloid deposits in the brain, where histopathological studies indicate higher density of PrP amyloid plaques in GSS than in familial CJD [1]. In the present study, the findings in two sporadic CJD patients showing no obvious [^{11}C]BF-227 retention in the brain additionally support this speculation. The difference may also be attributable to higher binding affinity of BF-227 to PrP amyloid cores compared to FDDNP and PIB. To clarify this, further in vitro studies comparing the binding affinities of different amyloid tracers to PrP plaques in TSE brain homogenates are needed.

The youngest GSS patient (GSS3) showed BF-227 retention in the cerebellum and thalamus but not in the neocortex. The clinical symptoms in this patient were consistent with the brain distribution of BF-227, with the patient presenting with severe gait disturbance and slurred speech resulting from cerebellar ataxia but no signs of cognitive impairment, suggesting a close relationship between PrP plaque deposition as measured by BF-227 and regional brain dysfunction. There are variations of clinical phenotypes in GSS [1, 3]. Such variations are yet to be explained; however, the pattern of regional PrP amyloid distribution might be one of the factors affecting clinical phenotypes of GSS. In vivo PrP amyloid imaging using [^{11}C]BF-227 or other PET tracers will clarify neuropathological aspects of clinical variations in GSS.

In summary, we confirmed binding of BF-227 to PrP plaques in vitro and in vivo. A clinical PET study using [^{11}C]BF-227 demonstrated in vivo detection of PrP amyloid plaques in GSS patients. This imaging technique provides a potential means of facilitating both early diagnosis and non-invasive disease monitoring of certain forms of TSEs because, despite a lack of selectivity for PrP, brain retention of BF-227 in GSS shows a distinct pattern of regional distribution than that usually observed in sporadic AD.

Acknowledgment We appreciate the assistance of Dr. S. Watanuki, Dr. M. Miyake and Dr. H. Takashima in the clinical PET studies. This study was supported in part by the Program for the Promotion of Fundamental Studies in Health Science of the NIBIO in Japan, Industrial Technology Research Grant Program of the NEDO in Japan, and Health and Labor Sciences Research Grants (Translational Research and Research on Measures for Intractable Diseases) from the Ministry of Health, Labor, and Welfare of Japan.

References

1. DeArmond SJ, Kretzschmar HA, Prusiner SB. Prion diseases. In: Graham DI, Lantos PL, editors. Greenfield's neuropathology, 7th ed. London: Hodder Arnold. p. 273–323.
2. Collins SJ, Lawson VA, Masters CL. Transmissible spongiform encephalopathies. Lancet 2004;363:51–61.
3. Collins S, McLean CA, Masters CL. Gerstmann-Sträussler-Scheinker syndrome, fatal familial insomnia, and kuru: a review of these less common human transmissible spongiform encephalopathies. J Clin Neurosci 2001;8:387–97.
4. Noguchi-Shinohara M, Hamaguchi T, Kitamoto T, Sato T, Nakamura Y, Mizusawa H, et al. Clinical features and diagnosis of dura mater graft associated Creutzfeldt Jakob disease. Neurology 2007;69:360–7.
5. Lasmézas CI, Deslys JP, Demaimay R, Adjou KT, Hauw JJ, Dormont D. Strain specific and common pathogenic events in murine models of scrapie and bovine spongiform encephalopathy. J Gen Virol 1996;77(Pt 7):1601–9.
6. Schulz-Schaeffer WJ, Tschöke S, Kranefuss N, Dröse W, Hause-Reitner D, Giese A, et al. The paraffin-embedded tissue blot detects PrP(Sc) early in the incubation time in prion diseases. Am J Pathol 2000;156:51–6.
7. Fraser JR. What is the basis of transmissible spongiform encephalopathy induced neurodegeneration and can it be repaired? Neuropathol Appl Neurobiol 2002;28:1–11.
8. Small GW, Kepe V, Ercoli LM, Siddarth P, Bookheimer SY, Miller KJ, et al. PET of brain amyloid and tau in mild cognitive impairment. N Engl J Med 2006;355:2652–63.
9. Klunk WE, Engler H, Nordberg A, Wang Y, Blomqvist G, Holt DP, et al. Imaging brain amyloid in Alzheimer's disease with Pittsburgh Compound-B. Ann Neurol 2004;55:306–19.
10. Verhoeff NP, Wilson AA, Takeshita S, Trop L, Hussey D, Singh K, et al. In-vivo imaging of Alzheimer disease beta-amyloid with [11C]SB-13 PET. Am J Geriatr Psychiatry 2004;12:584–95.
11. Rowe CC, Ackerman U, Browne W, Mulligan R, Pike KL, O'Keefe G, et al. Imaging of amyloid beta in Alzheimer's disease with 18F-BAY94–9172, a novel PET tracer: proof of mechanism. Lancet Neurol 2008;7:129–35.
12. Kudo Y, Okamura N, Furumoto S, Tashiro M, Furukawa K, Maruyama M, et al. 2-(2-[2-Dimethylaminothiazol-5-yl]ethenyl)-6-(2-[fluoro]ethoxy)benzoxazole: a novel PET agent for in vivo detection of dense amyloid plaques in Alzheimer's disease patients. J Nucl Med 2007;48:553–61.
13. Ishikawa K, Doh-ura K, Kudo Y, Nishida N, Murakami-Kubo I, Ando Y, et al. Amyloid imaging probes are useful for detection of prion plaques and treatment of transmissible spongiform encephalopathies. J Gen Virol 2004;85:1785–90.
14. Bresjanac M, Smid LM, Vovko TD, Petric A, Barrio JR, Popovic M. Molecular-imaging probe 2-(1-[6-[(2-fluoroethyl)(methyl) amino]-2-naphthyl]ethylidene) malononitrile labels prion plaques in vitro. J Neurosci 2003;23:8029–33.
15. Sadowski M, Pankiewicz J, Scholtzova H, Tsai J, Li Y, Carp RI, et al. Targeting prion amyloid deposits in vivo. J Neuropathol Exp Neurol 2004;63:775–84.
16. Hoefert VB, Aiken JM, McKenzie D, Johnson CJ. Labeling of the scrapie-associated prion protein in vitro and in vivo. Neurosci Lett 2004;371:176–80.
17. Boxer AL, Rabinovici GD, Kepe V, Goldman J, Furst AJ, Huang SC, et al. Amyloid imaging in distinguishing atypical prion disease from Alzheimer disease. Neurology 2007;69:283–90.
18. Villemagne VL, McLean CA, Reardon K, Boyd A, Lewis V, Klug G, et al. 11C-PiB PET studies in typical sporadic Creutzfeldt-Jakob disease. J Neurol Neurosurg Psychiatry 2009;80:998–1001. doi:10.1136/jnnp.2008.171496.
19. Okamura N, Suemoto T, Shimadzu H, Suzuki M, Shiomitsu T, Akatsu H, et al. Styrylbenzoxazole derivatives for in vivo imaging of amyloid plaques in the brain. J Neurosci 2004;24:2535–41.
20. Ishikawa K, Kudo Y, Nishida N, Suemoto T, Sawada T, Iwaki T, et al. Styrylbenzoazole derivatives for imaging of prion plaques and treatment of transmissible spongiform encephalopathies. J Neurochem 2006;99:198–205.

21. Waragai M, Okamura N, Furukawa K, Tashiro M, Furumoto S, Funaki Y, et al. Comparison study of amyloid PET and voxel-based morphometry analysis in mild cognitive impairment and Alzheimer's disease. J Neurol Sci 2009;285:100–8. doi:10.1016/j.jns.2009.06.005.
22. Okamura N, Furumoto S, Funaki Y, Suemoto T, Kato M, Ishikawa Y, et al. Binding and safety profile of novel benzoxazole derivative for in vivo imaging of amyloid deposits in Alzheimer's disease. Geriatr Gerontol Int 2007;7:393–400.
23. Zeidler M, Gibbs CJ Jr, Meslin F. WHO manual for strengthening diagnosis and surveillance of Creutzfeldt-Jakob disease. Geneva: World Health Organization; 1998. p. 47–51.
24. McKhann G, Drachman D, Folstein M, Katzman R, Price D, Stadlan EM. Clinical diagnosis of Alzheimer's disease: report of the NINCDS-ADRDA Work Group under the auspices of Department of Health and Human Services Task Force on Alzheimer's Disease. Neurology 1984;34:939–44.
25. Friston KJ, Holmes AP, Worsley KJ, Poline JP, Frith CD, Frackowiack RSJ. Statistical parametric maps in functional imaging: a general linear approach. Hum Brain Mapp 1995;2:189–210.
26. Masters CL, Gajdusek DC, Gibbs CJ Jr. Creutzfeldt-Jakob disease virus isolations from the Gerstmann-Sträussler syndrome with an analysis of the various forms of amyloid plaque deposition in the virus-induced spongiform encephalopathies. Brain 1981;104:559–88.
27. Ironside JW, McCardle L, Horsburgh A, Lim Z, Head MW. Pathological diagnosis of variant Creutzfeldt-Jakob disease. APMIS 2002;110:79–87.
28. Hill AF, Zeidler M, Ironside J, Collinge J. Diagnosis of new variant Creutzfeldt-Jakob disease by tonsil biopsy. Lancet 1997;349:99–100.
29. Doh-ura K, Ishikawa K, Murakami-Kubo I, Sasaki K, Mohri S, Race R, et al. Treatment of transmissible spongiform encephalopathy by intraventricular drug infusion in animal models. J Virol 2004;78:4999–5006.
30. Rainov NG, Tsuboi Y, Krolak-Salmon P, Vighetto A, Doh-Ura K. Experimental treatments for human transmissible spongiform encephalopathies: is there a role for pentosan polysulfate? Expert Opin Biol Ther 2007;7:713–26.
31. De Luigi A, Colombo L, Diomede L, Capobianco R, Mangieri M, Miccolo C, et al. The efficacy of tetracyclines in peripheral and intracerebral prion infection. PLoS One 2008;3:e1888.
32. Teruya K, Kawagoe K, Kimura T, Chen CJ, Sakasegawa Y, Doh-ura K. Amyloidophilic compounds for prion diseases. Infect Disord Drug Targets 2009;9:15–22.
33. Forloni G, Salmona M, Marcon G, Tagliavini F. Tetracyclines and prion infectivity. Infect Disord Drug Targets 2009;9:23–30.

J Neurol (2010) 257:721–727
DOI 10.1007/s00415-009-5396-8

ORIGINAL COMMUNICATION

Amyloid PET in mild cognitive impairment and Alzheimer's disease with BF-227: comparison to FDG–PET

Katsutoshi Furukawa · Nobuyuki Okamura · Manabu Tashiro · Masaaki Waragai · Shozo Furumoto · Ren Iwata · Kazuhiko Yanai · Yukitsuka Kudo · Hiroyuki Arai

Received: 6 June 2009 / Revised: 29 August 2009 / Accepted: 10 November 2009 / Published online: 28 November 2009

Abstract We recently developed a novel PET tracer, ^{11}C-labeled 2-(2-[2-dimethylaminothiazol-5-yl]ethenyl)-6-(2-[fluoro]ethoxy)benzoxazole ([^{11}C]BF-227), and had success with in vivo detection of amyloid plaques in Alzheimer's disease (AD) brains (Kudo et al. in J Nucl Med 8:553–561, 2007). We applied this tracer to subjects with mild cognitive impairment (MCI) and AD in order to elucidate the status of amyloid plaque deposition in MCI and compared the diagnostic performance of BF-227-PET with that of FDG–PET in AD cases. We studied 12 aged normal (AN) subjects, 15 MCIs and 15 ADs with PET using [^{11}C]BF-227. PET images were obtained after administration of BF-227 and the regional standardized uptake value (SUV) and the ratio of regional to cerebellar SUV were calculated as an index of BF-227 binding. AD patients showed increased uptake of [^{11}C]BF-227 in the neocortical areas and striatum as well as decreased glucose metabolism in temporoparietal, posterior cingulate and medial temporal areas. MCI subjects showed a significant increase in BF-227 uptake in the neocortical areas similar to AD, and the most significant difference of BF-227 retention was observed in the parietal lobe if its retentions for MCI were compared to those for AD and AN. On the other hand, glucose hypometabolism in MCI was confined to cingulate and medial temporal cortices. Neocortical BF-227 uptake negatively correlated with glucose metabolism. Receiver operating characteristic (ROC) analysis indicated higher specificity and sensitivity with BF-227-PET than those with FDG–PET for differential diagnosis between AD and normal control. We conclude that [^{11}C]BF-227-PET has a possibility to be a useful technology for early detection of AD pathology and also even in the MCI stage.

Keywords Alzheimer's disease · Amyloid · Senile plaque · PET · MCI

K. Furukawa and N. Okamura equally contributed to the article.

K. Furukawa (✉) · M. Waragai · H. Arai
Department of Geriatrics and Gerontology,
Division of Brain Sciences, Institute of Development,
Aging and Cancer, Tohoku University,
4-1 Seiryomachi, Aobaku, Sendai 980-8498, Japan
e-mail: kfurukawa-ns@umin.ac.jp

N. Okamura · S. Furumoto · K. Yanai
Department of Pharmacology,
Tohoku University Graduate School of Medicine,
4-1 Seiryomachi, Aobaku, Sendai 980-8575, Japan

M. Tashiro
Division of Cyclotron Nuclear Medicine,
Cyclotron and Radioisotope Center, 6-3Aoba,
Aramaki, Aoba-ku, Sendai, Miyagi 980-8578, Japan

R. Iwata
Division of Radiopharmaceutical Chemistry,
Cyclotron and Radioisotope Center, 6-3Aoba,
Aramaki, Aoba-ku, Sendai, Miyagi 980-8578, Japan

Y. Kudo
Department of NeuroImaging Research,
Innovation New Biomedical Engineering Center,
Tohoku University, 4-1 Seiryomachi, Aobaku,
Sendai 980-8498, Japan

Introduction

Senile or amyloid plaque is a pathological hallmark of Alzheimer's disease (AD), and amyloid β peptide (Aβ), which is a main component of the senile plaque, is believed to play a key role in the pathogenesis of AD [8]. In recent years several laboratories, including ours, have succeeded in visualizing Aβ deposition in living patients' brains with

AD using PET probes [13, 14, 24]. Pittsburgh Compound-B (PIB), which is the most commonly used probe for Aβ now, has been applied not only to AD but also to several other neurological disorders [15, 24].

Petersen from the Mayo clinic addressed the concept of mild cognitive impairment (MCI), which is an intermediate state between normal aging and AD [20, 21]. The criteria he stated for MCI are cognitive concern expressed by a physician, informant, participant or nurse; cognitive impairment in one or multiple domains (executive function, memory, language or visuospatial); normal functional activities; not demented.

Regional cerebral glucose metabolism (rCMRglu) has been studied by several investigators [9, 18, 19] using [^{18}F] 2-fluoro-deoxy-D-glucose (FDG) and PET in diseases causing dementia including AD. We used BF-227-PET as well as FDG–PET on the same subjects (AN, MCI, and AD) and carefully analyzed and compared the results with these two kinds of PET. Finally using these data we investigated and compared the specificity and sensitivity of BF-227 PET and FDG–PET in diagnosing AD.

Method

Twelve ANs, 15 subjects with MCI and 15 patients with AD were recruited in the present study. The demographic information of the subjects is shown in Table 1. The diagnosis for MCI and probable AD followed the MCI clinical criteria presented by "Petersen et al." [20] and "the National Institute of Neurological and Communicative Disorders and Stroke—Alzheimer's Disease and Related Disorders Association" [17], respectively. In 15 MCI subjects, 10 were amnestic multi-domain MCI and the other 5 subjects were amnestic single-domain MCI. Mini-mental state examination (MMSE) scores were significantly different between "AN and MCI", "AN and AD", and "MCI and AD". The study protocol was approved by the Committee on Clinical Investigation at Tohoku University School of Medicine and the Advisory Committee on Radioactive Substances at Tohoku University. After a complete description of the study to the patients and subjects, written informed consent was obtained.

Table 1 Demographic details of the subjects in this study

	N	Gender	Age	MMSE
AN	12	M/F = 7/5	66.3 ± 3.3	29.9 ± 0.3
MCI	15	M/F = 8/7	78.3 ± 3.8	25.5 ± 2.5
AD	15	M/F = 5/10	72.5 ± 6.9	19.5 ± 3.7

AN aged normal, *MCI* mild cognitive impairment, *AD* Alzheimer's disease. MMSE scores are significantly different between "AN and MCI", "AN and AD", and "MCI and AD"

The PET procedure for BF-227 was described precisely before [14]. BF-227 and its *N*-desmethylated derivative (a precursor of [^{11}C]BF-227) were custom-synthesized by Tanabe R&D Service Co. [^{11}C]BF-227 was synthesized from the precursor by *N*-methylation in dimethyl sulfoxide using [^{11}C]methyl triflate. The [^{11}C]BF-227 PET study was performed using a PET SET-2400 W scanner (Shimadzu Inc., Japan). After intravenous injection of 211–366 mBq of [^{11}C]BF-227, dynamic PET images were obtained for 60 min with each subject's eyes closed. Standardized uptake value (SUV) images of [^{11}C]BF-227 were obtained by normalizing tissue radioactivity concentration by injected dose and body weight. The FDG–PET procedure was described previously [19]. Subjects were scanned in a quiet and dimly-lit room with their eyes closed after at least 4 h of food restriction. Following a 68 Ga/Ga transmission scan of 7 min duration, an emission scan, which lasted 60 min after intravenous injection of FDG, was performed. The emission data were corrected for tissue attenuation using the transmission data. Regions of interest (ROIs) were placed on individual axial magnetic resonance (MR) images in the cerebellar hemisphere, striatum, frontal, lateral temporal, medial temporal, parietal, occipital, anterior and posterior cingulate cortices. The ROI information was then copied onto dynamic PET SUV images, and regional SUVs were sampled using Dr. View/LINUX software (AJS inc., Japan). Because there were neither senile plaques nor glucose hypometabolism in the cerebellum of AD, ratios of regional SUV to cerebellar SUV (SUVR) were calculated as an index of [^{11}C]BF-227 retention and CMRglu. Neocortical SUVR was calculated by averaging SUVRs in the frontal, lateral temporal, parietal and posterior cingulate cortices.

For statistical comparison in the three groups, we applied one-way analysis of variance (ANOVA) followed by the Bonferroni-Dunn post hoc test. The performance of diagnostic indices to discriminate among groups was assessed using the ROC analysis. Areas under ROC curves (AUC) were calculated and compared using GraphPad Prism Software (GraphPad Software Inc., San Diego, CA). Statistical significance was defined as $p < 0.05$.

Results

BF-227 retention in MCI

First, we analyzed PET images with [^{11}C]BF-227 among the three groups (AN, MCI, and AD), and representative brain PET images are shown in Fig. 1. As indicated in the figure, some MCI subjects showed strong retention of [^{11}C]BF-227, but other MCI subjects did not. Most AD cases, however, indicated strong accumulation of [^{11}C]BF-227 especially in

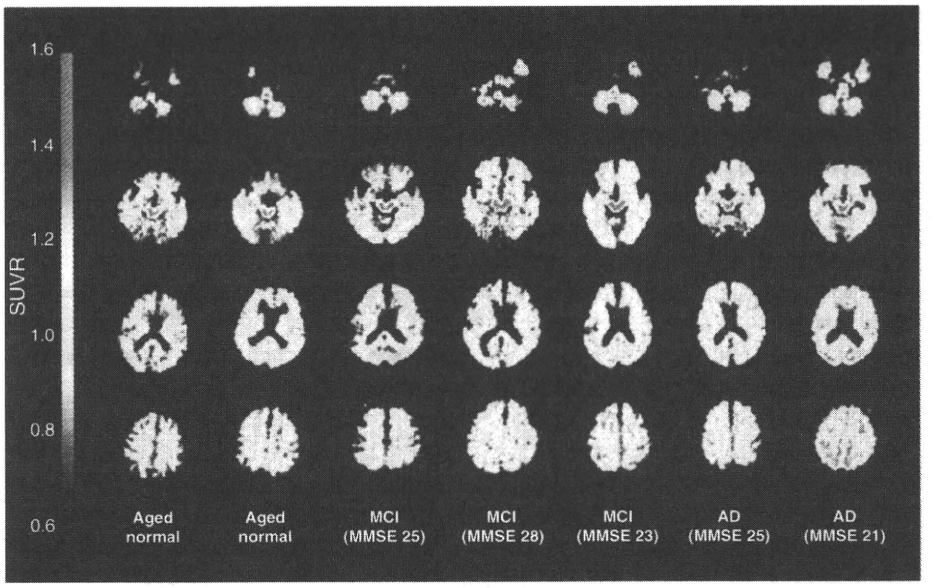

Fig. 1 Representative axial brain PET images with BF-227. Both the AD cases showed high SUVR compared to the aged normal subjects, although the MCI cases showed heterogeneity, that is, one MCI case (MMSE = 25) showed a comparative SUVR level to AN but another case showed SUVR as high as the AD level

frontal, temporal and parietal cortices. If the retention pattern of [^{11}C]BF-227 is compared to that of PIB, the accumulation of [^{11}C]BF-227 in the frontal lobe looks much weaker than that of PIB [3].

Figure 2 shows the mean neocortical and regional SUVRs of [^{11}C]BF-227 for the three groups. Both the mean neocortical SUVRs for MCI and AD are significantly higher than that for AN. As we previously reported [1], significantly higher SUVRs were observed in most cerebral regions in AD compared to AN except for the medial temporal lobe. MCI subjects indicated a significantly increased SUVR in frontal, lateral temporal, parietal, occipital cortices as well as anterior cingulate gyrus compared to AN, and the most prominent increase was observed in the lateral temporal cortex. A significantly lower SUVR in MCI was observed in the parietal cortex compared to AD. In the other neocortical regions, MCI subjects showed a tendency towards milder retention of BF-227 than that in AD. In the relationship between BF retentions and MMSE scores in all the subjects together (NC, MCI, and AD), no strong correlations were observed (data not shown).

Cerebral glucose metabolism in AN, MCI and AD

Next, we analyzed CMRglu in the same subjects using FDG–PET in order to compare to the findings with [^{11}C]BF-227, which is considered to indicate amyloid plaque depositions. As a result, a significant reduction of neocortical SUVR was observed in both MCI and AD patients compared to AN in FDG–PET (Table 1; Fig. 3). Regional SUVR in FDG–PET was significantly decreased in the cingulate gyrus and medial temporal cortex of MCI subjects and in the lateral temporal, parietal, posterior cingulate and medial temporal cortices of AD patients, compared to AN. Table 2.

Neocortical SUVR of FDG–PET for each subject was plotted against neocortical SUVR of BF-227-PET (Fig. 4a). SUVR of BF-227 negatively correlated to SUVR of FDG in analyzing the subjects from three groups all together ($r = -0.337$, $p = 0.029$). A significant correlation of regional SUVR in BF-227-PET and FDG–PET was also observed in the temporal and parietal cortices (data not shown). However, no significant correlation was observed when the analysis was confined to the subjects in each group.

Furthermore, in order to compare sensitivity and specificity to differentiate AD from AN, ROC analysis was performed for the lateral temporal SUVR of BF-227 and posterior cingulate SUVR of FDG (Fig. 4b). The AUC for BF-227 (0.994) is much higher than that for FDG (0.839), indicating that BF-227 is more sensitive as well as more specific than FDG in diagnosing AD.

Discussion

Our group recently developed a novel PET tracer, BF-227, and has reported that this compound is able to selectively detect dense amyloid deposits including senile plaques primarily in the posterior association area of AD patients. In the present study we applied this tracer to MCI cases and concluded that the mean value for the MCI cases with BF-227 was intermittent between AN and AD. Also we clarified that BF-227-PET is a useful technology to distinguish early AD patients from AN compared to FDG–PET.

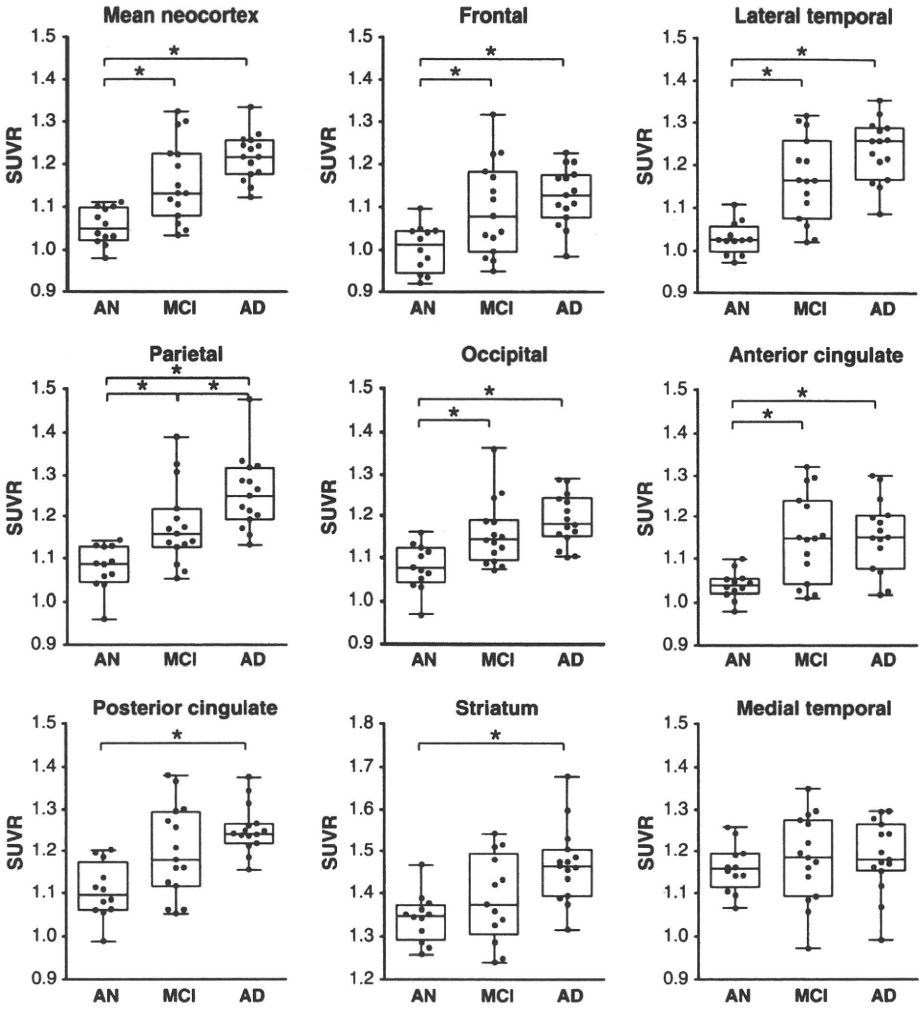

Fig. 2 Box plots of SUVR values with BF-227 PET for AN, MCI and AD. Each *dot* indicates the mean SUVR from "the mean neocortex" and "the eight regions", that is, frontal, temporal, parietal, occipital, anterior cingulate, posterior cingulated, striatum and medial temporal cortex. *Box* indicates interquartile range. *Vertical bars* indicate minimum–maximum range

MCI is now classified into 4 subtypes, that is, amnestic single-domain MCI, amnestic multi-domain MCI, non-amnestic single-domain MCI and non-amnestic multi-domain MCI. The important thing is that MCI (especially amnestic MCI) is regarded as a prodromal state of AD, in other words, a high percentage of MCI subjects are considered to convert to AD. It has been reported that 10–20% of MCI cases are going to convert to AD although only 1–2% of normal elderly convert to AD [21]. The present study concludes that MCI has high levels of [^{11}C]BF-227 retention indicating that senile plaque deposition already advances severely in the stage of MCI before dementia symptoms become obvious. Previous amyloid PET studies using ^{18}F-labeled 2-(1,1-dicyano-propen-2-yl)-6-(2-fluoroethyl)-methylamino-naphthalene (FDDNP) or PIB also indicated significant tracer retention in MCI and AD. Small et al. [24] presented that FDDNP can detect a high signal in MCI by binding not only for amyloid plaques but also tau neurofibrillary tangles, and the retention level for MCI is between AN and AD. On the other hand, several groups reported that about a half of the MCI subjects showed PIB uptake in the AD range, and other MCI subjects indicated retention levels lower than the AD range [12]. A group from Sweden concluded that MCI subjects who converted to AD later showed significantly higher PIB retention compared to non-converting MCI subjects and NC [6]. The present study also revealed higher retention of BF-227 in 60–70% of MCI subjects and in almost all the AD patients. Therefore, the amyloid PET technique is considered to be a highly useful and strong method for early detection of AD patients in the MCI stage. These pieces of information are indispensable in applying new treatment technologies against dementia into the prodromal stage of Alzheimer's disease. In other words, because it is considered that aggregation and deposition of Aβ starts much earlier before patients indicate symptoms of dementia, it is undoubtedly important to detect Aβ deposition as early as

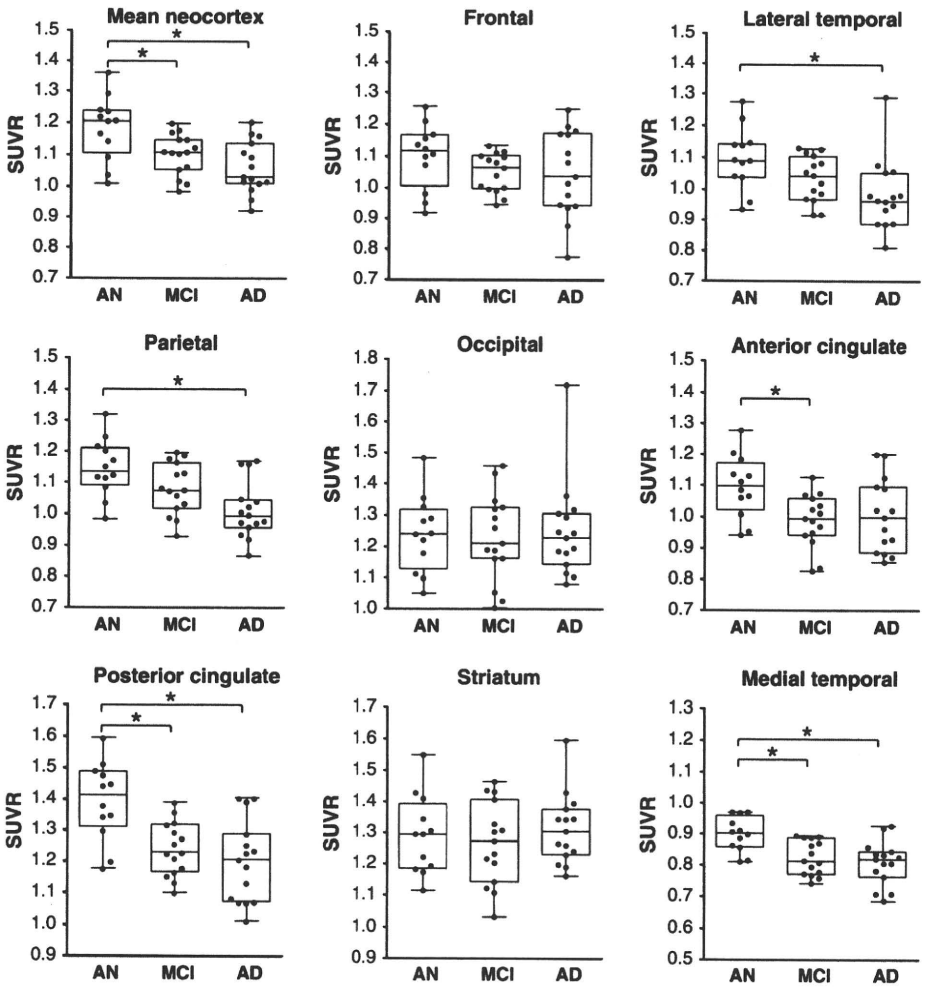

Fig. 3 Box plots of SUVR values with FDG–PET for AN, MCI and AD. Each *dot* indicates the mean SUVR from the mean neocortex and eight cerebral regions, that is, frontal, temporal, parietal, occipital, anterior cingulate, posterior cingulated, striatum and medial temporal cortex. *Boxes* indicate interquartile range. *Vertical bars* indicate minimum–maximum range

Table 2 Comparison of SUVR values of BF-227-PET and FDG–PET

		Mean neo cortex	Frontal	Lateral temporal	Parietal	Occipital	Anterior cingulate	Posterior cingulate	Striatum	Medial temporal
BF-227	AN	1.05 ± 0.04	1.00 ± 0.06	1.03 ± 0.04	1.08 ± 0.05	1.08 ± 0.05	1.04 ± 0.03	1.11 ± 0.07	1.34 ± 0.06	1.16 ± 0.06
	MCI	1.16 ± 0.10*	1.10 ± 0.11*	1.17 ± 0.10*	1.18 ± 0.10*	1.16 ± 0.08*	1.15 ± 0.11*	1.20 ± 0.11	1.41 ± 0.11	1.18 ± 0.10
	AD	1.22 ± 0.06*	1.13 ± 0.07*	1.24 ± 0.07*	1.25 ± 0.09*†	1.19 ± 0.06*	1.16 ± 0.09*	1.25 ± 0.06*	1.47 ± 0.09*	1.19 ± 0.09
FDG	AN	1.18 ± 0.10	1.10 ± 0.11	1.10 ± 0.10	1.15 ± 0.09	1.24 ± 0.12	1.10 ± 0.10	1.39 ± 0.13	1.29 ± 0.13	0.90 ± 0.06
	MCI	1.10 ± 0.06*	1.05 ± 0.06	1.03 ± 0.07	1.08 ± 0.08	1.23 ± 0.14	0.99 ± 0.08*	1.24 ± 0.09*	1.27 ± 0.13	0.82 ± 0.06*
	AD	1.06 ± 0.08*	1.05 ± 0.14	0.98 ± 0.11*	1.01 ± 0.09*	1.25 ± 0.15	1.00 ± 0.12	1.20 ± 0.13*	1.31 ± 0.11	0.81 ± 0.07*

Mean SUVR value for each brain region was obtained from AN, MCI and AD. * $p < 0.05$, versus AN, † $p < 0.05$ versus MCI

possible in order to begin medication to prevent or treat cognitive decline before the manifestations of dementia become clear.

In most PIB positive MCI and AD cases presented by several different laboratories, the frontal cortex showed high PIB retention, although the frontal cortex is not a region where amyloid plaques are predominantly rich in the early stage of AD or MCI according to the autopsy studies [1, 10]. Our newly developed tracer, BF-227, showed relatively high retention in temporal and parietal lobes for MCI and AD compared to the results with PIB. Since it is well known that the functional activity of the parietal lobe decreases in the early stage of AD [16], it is reasonable that the distribution of high BF-227-PET

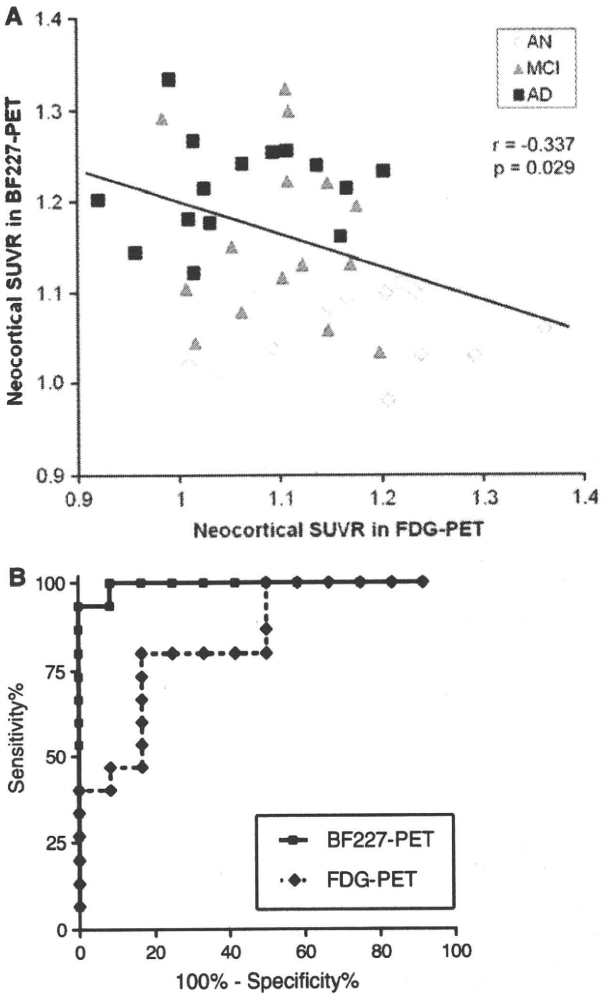

Fig. 4 **a** Relationship between neocortical SUVRs in FDG–PET and BF-227-PET. Neocortical SUVR of FDG–PET for each subject was plotted against neocortical SUVR of BF-227-PET. White, gray and black dots indicate AN, MCI and AD, respectively. **b** Receiver operating characteristic (ROC) curves of BF-227 and FDG–PET. BF-227-PET SUVR in the lateral temporal cortex and FDG–PET SUVR in the posterior cingulate cortex for differentiation between AD and AN

retention is closely related to the area indicating functional deterioration in the early stage of AD or MCI.

Low rCMRglu in AD especially in the posterior cingulate, precuneus, temporoparietal and frontal cortices was reported. FDG–PET has also been used in investigations for MCI, and low rCMRglu in the temporo-parietal and medial frontal cortices and hippocampus was reported as the most prominent predictor of subsequent cognitive decline [2–5]. Our results indicate, however, that amyloid retention detected by BF-227 is more sensitive and specific than FDG–PET for AD diagnosis. Therefore it is reasonable that amyloid PET is more sensitive than FDG–PET for detecting MCI, which is regarded as a prodromal state of dementia or early AD. According to previous autopsy studies with MCI, amyloid plaques were found predominantly in the temporal lobe structure and most amnestic MCI cases showed Braak stage II or III [11, 22]. Furthermore both neurofibrillary tangles and senile plaques were found in nondemented aging and "preclinical" AD, and profound neuronal loss was observed in layer II of the entorhinal cortex [7, 23]. Our results with BF-227 PET for MCI presented here agree with postmortem studies because BF-227 also showed high retention predominantly in the temporal lobe and the retention was intermittent between NC and AD. There are some discrepancies, however, between the results with our BF-227-PET and with autopsy, that is, some cerebral white matter, thalamus and pons showed high retention of BF-227 in MCI, although these regions are usually not rich in senile plaques in the autopsy studies. Although it is considered that the deposition of BF-227 in these regions comes from its non-specific retention by high lipophilicity, it is supposed that more precise studies are needed using more subjects for both PET and autopsy.

We now have to carefully consider the heterogeneity of BF-227 retention in MCI, which was also observed in FDDNP or PIB studies, that is, some subjects show rich retention but others do not. Although it was reported that MCI subjects showing high retention of PIB had a high tendency to convert to AD as we mentioned above [6], the number of subjects they examined was relatively small. Therefore, further careful studies are needed to clarify if the accumulation of amyloid PET probes correlates with the severity of cognitive impairment and a conversion rate to dementia.

Our results using BF-227 for MCI are "continuous" rather than "off/on", "negative/positive" or "dichotomous" signals compared to those with PIB. We speculate that because BF-227 can depict a small difference of amyloid deposition more finely than PIB, the results with BF-227 in MCI are more continuous than those with PIB. Therefore, BF-227 could reveal a degree of senile plaque deposition more precisely and accurately than PIB as far as in cases with MCI.

We would like to conclude that our newly developed amyloid PET tracer, BF-227, can detect amyloid aggregation and deposition in MCI cases and the PET signal intensity for MCI was intermittent between NC and AD. Results obtained with BF-227 PET are significantly more sensitive and specific than FDG–PET in diagnosing AD. As far as the retention pattern in the frontal and parietal cortices, BF-227 more accurately reflects senile plaque deposition observed in the autopsy studies than PIB does. Therefore, BF-227 PET should be an invaluable tool for diagnosis of AD in the early stage. Finally, we recently developed a novel probe, which has similar structure to BF-

227, labeled with F-18, and applied it to living humans. We have finished more than 20 cases so far and obtained similar results to BF-227.

Acknowledgments This study was supported by the Program for the Promotion of Fundamental Studies in Health Science by the National Institute of Biomedical Innovation, the Special Coordination Funds for Promoting Science and Technology, the Industrial Technology Research Grant Program from the New Energy and Industrial Technology Development Organization of Japan, Health and Labour Sciences Research Grants for Translational Research from the Ministry of Health, and the Ministry of Education, Culture, Sports and Technology. We appreciate technical assistance of Dr. Shoichi Watanuki and Dr. Yoichi Ishikawa in the clinical PET studies and Dr. Motohisa Kato in the imaging analysis.

References

1. Bennett DA, Cochran EJ, Saper CB, Leverenz JB, Gilley DW, Wilson RS (1993) Pathological changes in frontal cortex from biopsy to autopsy in Alzheimer's disease. Neurobiol Aging 14:589–596
2. Chételat G, Desgranges B, de la Sayette V, Viader F, Eustache F, Baron JC (2003) Mild cognitive impairment: Can FDG-PET predict who is to rapidly convert to Alzheimer's disease? Neurology 60:1374–1377
3. Chételat G, Eustache F, Viader F, De La Sayette V, Pélerin A, Mézenge F, Hannequin D, Dupuy B, Baron JC, Desgranges B (2005) FDG–PET measurement is more accurate than neuropsychological assessments to predict global cognitive deterioration in patients with mild cognitive impairment. Neurocase 11:14–25
4. de Leon MJ, Convit A, Wolf OT, Tarshish CY, DeSanti S, Rusinek H, Tsui W, Kandil E, Scherer AJ, Roche A, Imossi A, Thorn E, Bobinski M, Caraos C, Lesbre P, Schlyer D, Poirier J, Reisberg B (2001) Fowler et al. Prediction of cognitive decline in normal elderly subjects with 2-[(18)F]fluoro-2-deoxy-D-glucose/positron-emission tomography (FDG/PET). Proc Natl Acad Sci USA 98:10966–10971
5. Drzezga A, Lautenschlager N, Siebner H, Riemenschneider M, Willoch F, Minoshima S, Schwaiger M, Kurz A (2003) Cerebral metabolic changes accompanying conversion of mild cognitive impairment into Alzheimer's disease: a PET follow-up study. Eur J Nucl Med Mol Imaging 30:1104–1113
6. Forsberg A, Engler H, Almkvist O, Blomquist G, Hagman G, Wall A, Ringheim A, Långström B, Nordberg A (2008) A PET imaging of amyloid deposition in patients with mild cognitive impairment. Neurobiol Aging 29:1456–1465
7. Gómez-Isla T, Price JL, McKeel DW Jr, Morris JC, Growdon JH, Hyman BT (1996) Profound loss of layer II entorhinal cortex neurons occurs in very mild Alzheimer's disease. J Neurosci 16:4491–4500
8. Hardy J, Selkoe DJ (2002) The amyloid hypothesis of Alzheimer's disease: progress and problems on the road to therapeutics. Science 297:353–356
9. Herholz K, Carter SF, Jones M (2007) PET studies in dementia. Br J Radiol 80:S160–S167
10. Iwatsubo T, Odaka A, Suzuki N, Mizusawa H, Nukina N, Ihara Y (1994) Visualization of A beta 42(43) and A beta 40 in senile plaques with end-specific A beta monoclonals: evidence that an initially deposited species is A beta 42(43). Neuron 13:45–53
11. Jicha GA, Parisi JE, Dickson DW, Johnson K, Cha R, Ivnik RJ, Tangalos EG, Boeve BF, Knopman DS, Braak H, Petersen RC (2006) Neuropathologic outcome of mild cognitive impairment following progression to clinical dementia. Arch Neurol 63:674–681
12. Kemppainen NM, Aalto S, Wilson IA, Någren K, Helin S, Brück A, Oikonen V, Kailajärvi M, Scheinin M, Viitanen M, Parkkola R, Rinne JO (2007) PET amyloid ligand [11C]PIB uptake is increased in mild cognitive impairment. Neurology 68:1603–1606
13. Klunk WE, Engler H, Nordberg A, Wang Y, Blomqvist G, Holt DP, Bergström M, Savitcheva I, Huang GF, Estrada S, Ausén B, Debnath ML, Barletta J, Price JC, Sandell J, Lopresti BJ, Wall A, Koivisto P, Antoni G, Mathis CA, Långström B (2004) Imaging brain amyloid in Alzheimer's disease with Pittsburgh Compound-B. Ann Neurol 55:306–319
14. Kudo Y, Okamura N, Furumoto S, Tashiro M, Furukawa K, Maruyama M, Itoh M, Iwata R, Yanai K, Arai H (2007) 2-(2-[2-Dimethylaminothiazol-5-yl]ethenyl) -6-(2-[fluoro]ethoxy)benzoxazole: a novel PET agent for in vivo detection of dense amyloid plaques in Alzheimer's disease patients. J Nucl Med 8:553–561
15. Mathis CA, Klunk WE, Price JC, DeKosky ST (2005) Imaging technology for neurodegenerative diseases: progress toward detection of specific pathologies. Arch Neurol 62:196–200
16. Matsuda H (2007) Role of neuroimaging in Alzheimer's disease, with emphasis on brain perfusion SPECT. J Nucl Med 48:1289–1300
17. McKhann G, Drachman D, Folstein M, Katzman R, Price D, Stadlan EM (1984) Clinical diagnosis of Alzheimer's disease: report of the NINCDS-ADRDA Work Group under the auspices of Department of Health and Human Services Task Force on Alzheimer's Disease. Neurology 34:939–944
18. Minoshima S, Giordani B, Berent S, Frey KA, Foster NL, Kuhl DE (1997) Metabolic reduction in the posterior cingulate cortex in very early Alzheimer's disease. Ann Neurol 42:85–94
19. Okamura N, Arai H, Higuchi M, Tashiro M, Matsui T, Hu XS, Takeda A, Itoh M, Sasaki H (2001) [18F]FDG–PET study in dementia with Lewy bodies and Alzheimer's disease. Prog Neuropsychopharmacol Biol Psychiatry 25:447–456
20. Petersen RC, Smith GE, Waring SC, Ivnik RJ, Tangalos EG, Kokmen E (1999) Mild cognitive impairment: clinical characterization and outcome. Arch Neurol 56:303–308
21. Petersen RC (2004) Mild cognitive impairment as a diagnostic entity. J Intern Med 256:183–194
22. Petersen RC, Parisi JE, Dickson DW, Johnson K, Cha R, Ivnik RJ, Tangalos EG, Boeve BF, Knopman DS, Braak H, Petersen RC (2006) Neuropathologic features of amnestic mild cognitive impairment. Arch Neurol 63:665–672
23. Price JL, Morris JC (1999) Tangles and plaques in nondemented aging and "preclinical" Alzheimer's disease. Ann Neurol 45:358–368
24. Small GW, Kepe V, Ercoli LM, Siddarth P, Bookheimer SY, Miller KJ, Lavretsky H, Burggren AC, Cole GM, Vinters HV, Thompson PM, Huang SC, Satyamurthy N, Phelps ME, Barrio JR (2006) PET of brain amyloid and tau in mild cognitive impairment. N Engl J Med 355:2652–2663

Original Research Article

Dementia and Geriatric Cognitive Disorders

Dement Geriatr Cogn Disord 2010;30:101–111
DOI: 10.1159/000318754

Accepted: June 15, 2010
Published online: August 21, 2010

Voxel-Based Analysis of Amyloid Positron Emission Tomography Probe [^{11}C]BF-227 Uptake in Mild Cognitive Impairment and Alzheimer's Disease

He Shao[a] Nobuyuki Okamura[a] Kentaro Sugi[a] Shozo Furumoto[a, b] Katsutoshi Furukawa[d] Manabu Tashiro[c] Ren Iwata[b] Hiroshi Matsuda[g] Yukitsuka Kudo[f] Hiroyuki Arai[d] Hiroshi Fukuda[e] Kazuhiko Yanai[a]

[a]Department of Pharmacology, Tohoku University Graduate School of Medicine, and Divisions of [b]Radiopharmaceutical Chemistry and [c]Cyclotron Nuclear Medicine, Cyclotron and Radioisotope Center, Tohoku University, and Departments of [d]Geriatrics and Gerontology, Division of Brain Sciences, and [e]Nuclear Medicine and Radiology, Institute of Development, Ageing and Cancer, Tohoku University, and [f]Innovation of New Biomedical Engineering Center, Tohoku University, Sendai, and [g]Department of Nuclear Medicine, Saitama Medical University, International Medical Center, Saitama, Japan

Key Words
Alzheimer's disease · Mild cognitive impairment · Positron emission tomography · Amyloid

Abstract
Aim: To determine early brain changes in the distribution of an amyloid positron emission tomography (PET) probe, ^{11}C-labeled BF-227 or [^{11}C]BF-227, in order to accurately predict the progression of mild cognitive impairment (MCI) to Alzheimer's disease (AD). ***Patients and Methods:*** Amyloid plaque burden was evaluated using [^{11}C]BF-227 PET in AD, MCI and aged normal controls. A voxel-based analysis of [^{11}C] BF-227 PET images was performed to characterize the culprit brain lesion in patients with MCI who were destined to progress to AD, referred to as MCI converters (MCI-C). In addition, binding characteristics of BF-227 to amyloid deposits were examined using postmortem AD brain samples. ***Results:*** Voxel-based statistical analyses of the BF-227 PET images clearly demonstrated an abnormal distribution of BF-227 mainly in the posterior association area in MCI-C and patients with AD. BF-227 uptake in the lateral temporal cortex was consistently observed in almost all MCI-C and patients with AD, and it distinguished MCI-C from MCI nonconverters. BF-227 binding strongly correlated with dense amyloid-β protein plaque density, but not with diffuse plaque density in the frontal cortex. ***Conclusion:*** BF-227 uptake in the lateral temporal cortex is a reliable indicator that can be used for predicting prognosis in patients with MCI.

Introduction

Alzheimer's disease (AD) is considered as the most common cause of dementia in the elderly. Since the extensive deposition of extracellular senile plaques is one of the pathological hallmarks of AD, many researchers have examined these lesions to try and understand the pathogenesis of AD. In 1984, amyloid-β protein (Aβ) was iso-

KARGER

Fax +41 61 306 12 34
E-Mail karger@karger.ch
www.karger.com

1420–8008/10/0302–0101$26.00/0

Accessible online at:
www.karger.com/dem

Nobuyuki Okamura, MD, PhD
Department of Pharmacology, Tohoku University School of Medicine
2-1 Seiryo-machi, Aoba-ku
Sendai 980-8575 (Japan)
Tel. +81 22 717 8058, Fax +81 22 717 8060, E-Mail oka@mail.tains.tohoku.ac.jp

lated from cerebrovascular amyloidosis [1], and in the following year, it was isolated from amyloid plaques and neurofibrillary tangles [2, 3]. Senile plaques, which are mostly composed of Aβ, are believed to accumulate years before the onset of cognitive decline in AD [4]. Ten years ago, the concept of amnestic mild cognitive impairment (MCI) was introduced by the Mayo Clinic group. Amnestic MCI is now considered to be an intermediate predementia stage in patients with AD. Approximately 10–15% of patients with MCI develop AD [5, 6].

Positron emission tomography (PET) imaging using an amyloid-binding agent is a valid method for in vivo evaluation of Aβ plaque burden [7]. Several small molecular amyloid-binding agents have been designed for monitoring amyloid deposits in patients with MCI and AD and for evaluating the efficacy of antiamyloid therapy [8–12]. Furthermore, we have developed several benzoxazole derivatives as potential candidates for amyloid PET probes [13, 14]. A PET study using ^{11}C-labeled BF-227, or [^{11}C]BF-227, successfully detected amyloid plaques in living patients with AD [10]. Recent clinical studies have demonstrated neocortical [^{11}C]BF-227 uptake in patients with MCI [11, 15]. This finding suggests that neocortical [^{11}C]BF-227 uptake could be a potential biomarker for predicting progression from MCI to AD. In previous studies, analysis of PET images was mainly based on analysis of regions of interest (ROI). To eliminate any prior hypothesis about ROI selection, we performed voxel-based analyses of whole brain regions and made comparisons between MCI, AD and aged normal control groups. After [^{11}C]BF-227 PET scanning, we prospectively followed patients with MCI and investigated the relationship between initial BF-227 uptake and prognosis from MCI. The purpose of this study was to explore early changes in the process of amyloid plaque deposition in AD and understand the pattern of neocortical BF-227 distribution for accurate prediction of prognosis in the MCI stage.

Patients and Methods

Subjects and Patients

[^{11}C]BF-227 PET scans were performed on 12 aged normal controls, 19 probable patients with AD and 14 patients with MCI. The patients with AD were recruited via the Tohoku University Hospital Dementia Patients Registry, and the diagnosis was made according to the National Institute of Neurological and Communicative Diseases and Stroke/Alzheimer's Disease and Related Disorders Association criteria [16]. The patients with AD were divided into 2 groups according to their clinical severity: AD1 (Mini-Mental State Examination, MMSE, score ≥20) and AD2 (MMSE score <20). The diagnosis of amnestic MCI was made according to previously published criteria [5], which are as follows: (1) memory complaint, (2) normal activities of daily living, (3) normal general cognitive function, (4) abnormal memory for age, and (5) no sign of dementia. All patients with MCI underwent medical and neuropsychological reevaluation at approximately 3-month intervals and were divided into 2 groups: MCI converters (MCI-C; n = 7) and MCI nonconverters (MCI-NC; n = 7). MCI-C were defined as patients who eventually developed AD within a mean follow-up of 40.0 ± 6.9 months (range: 28–49 months), and MCI-NC were defined as patients having a transient memory loss or remaining cognitively stable for at least 3 years of follow-up (42.4 ± 2.2 months; range: 40–45 months). Aged volunteers who were taking no centrally active medication and who had no cognitive impairment or cerebrovascular lesion on MRI images were recruited as aged normal controls. All aged normal controls were screened via their medical history and responses to the MMSE. Subjects with medical conditions such as multiple cerebral infarctions, normal-pressure hydrocephalus, subdural hematoma, brain tumor, epilepsy, major depression, Parkinson's disease and other neurodegenerative diseases were excluded. In addition, asymptomatic cerebral infarction was not detected on T_2-weighted MRI images in the aged normal controls. The demographic data for all patients and aged normal controls are shown in table 1. The protocol of this study was approved by the Committee on Clinical Investigation at the Tohoku University School of Medicine, and by the Advisory Committee on Radioactive Substances at Tohoku University. Written informed consent was obtained from all patients and controls after complete description of the study. The clinical study was performed in accordance with the Declaration of Helsinki.

Radiosynthesis

BF-227 and its N-desmethylated derivative, a precursor to [^{11}C]BF-227, were synthesized by Tanabe R&D Service Co. (Osaka, Japan). [^{11}C]BF-227 was synthesized from the precursor by N-methylation in dimethyl sulfoxide, using [^{11}C]methyl triflate [10]. After quenching the reaction with 5% acetic acid in ethanol, [^{11}C]BF-227 was separated from the crude mixture by semipreparative, reversed-phase high-performance liquid chromatography and isolated from the collected fraction by solid-phase extraction. Purified [^{11}C]BF-227 was solubilized in isotonic saline containing 1% polysorbate 80 and 5% ascorbic acid. The saline solution was filter sterilized with a 0.22-μm Millipore filter (Millipore Co., Bedford, Mass., USA) for clinical use. At the end of synthesis, the radiochemical yields were greater than 50%, based on [^{11}C]methyl triflate, and the specific radioactivity ranged from 119 to 138 GBq/μmol. Radiochemical purities were greater than 95%.

Scanning Protocol

The [^{11}C]BF-227 PET study was performed using a SET-2400W PET scanner (Shimadzu, Kyoto, Japan). After intravenous injections of 211–366 MBq [^{11}C]BF-227, dynamic PET images were obtained for 60 min (23 sequential scans; 5 scans × 30 s, 5 scans × 60 s, 5 scans × 150 s, and 8 scans × 300 s) with closed eyes. All aged normal controls and patients underwent MRI using a 1.5-tesla MRI scanner (GE Signa Hispeed; GE Healthcare, Milwaukee, Wisc., USA). A 3-D volumetric acquisition of a T_1-weighted gradient echo sequence produced a gapless series of thin axial sections, using a vascular time-of-flight spoiled gradient echo sequence

Table 1. Demographic information on all the subjects

	Aged normal	MCI-NC	MCI-C	AD1	AD2	All AD
Number	12	7	7	10	9	19
Age, years	67.3 ± 2.7 (64–71)	77.6 ± 3.1* (74–82)	79.4 ± 4.2* (75–85)	72.9 ± 5.4 (65–85)	72.6 ± 7.3 (61–82)	72.7 ± 6.2 (61–85)
Gender (F/M), n	6/6	5/2	3/4	2/8	4/5	6/13
MMSE score	29.9 ± 0.3 (29–30)	26.3 ± 1.1 (25–28)	24.6 ± 3.4 (23–29)	22.7 ± 1.4* (21–25)	17.2 ± 2.9*,# (12–20)	20.1 ± 3.6 (12–25)
Years of education	13.2 ± 0.94	12.3 ± 0.48	11.9 ± 0.55	10.9 ± 0.72	10.3 ± 0.65	10.5 ± 0.42
GDS score	4.01 ± 0.44	4.32 ± 0.34	4.79 ± 0.31	4.23 ± 0.35	4.18 ± 0.46	4.20 ± 0.28

Values denote means ± SD with ranges in parentheses unless stated otherwise. Kruskal-Wallis test followed by Dunn's multiple comparison test. GDS = Geriatric Depression Scale. * $p < 0.05$ versus aged normal, # $p < 0.05$ versus MCI-NC.

(echo time/repetition time: 2.4/50 ms; flip angle: 45°; acquisition matrix: 256 × 256; 1 excitation; field of view: 22 cm; slice thickness: 2.0 mm).

Image Analysis

Standardized uptake value (SUV) images of [^{11}C]BF-227 were obtained by normalizing tissue concentration to injected dose and body weight. Average summations of SUV images were created from frames (20–40 min after injection) of dynamic PET images. Individual MR images were anatomically correlated with BF-227 PET images, using a statistical parametric mapping software (SPM5; Wellcome Department of Imaging Neuroscience, London, UK) [17]. ROI in the frontal cortex (Brodmann's areas, BA, 8, 9, 10, 44, 45, 46 and 47), lateral temporal cortex (BA 21, 22, 37 and 38), parietal cortex (BA 39 and 40), occipital cortex (BA 17), posterior cingulate cortex (BA 31) and cerebellar hemisphere were superimposed on MRI images, as described previously [10]. ROI information was then copied onto PET images, and regional SUV values at 20–40 min after injection were sampled using Dr. View/LINUX software (AJS, Tokyo, Japan). The cerebellum was used as the reference region. The regional-to-cerebellum SUV ratio (SUVR) was calculated and used as an index of BF-227 retention because the cerebellum is reported to be a region free of fibrillar amyloid plaques in the AD brain. Voxel-by-voxel comparisons between images from aged normal controls, patients with MCI and patients with AD were performed using SPM5 software. Spatial normalization was performed using an MR T_1 template of SPM5 to transfer PET images onto a standard stereotactic space. The normalized PET images were smoothed, using a 12 × 12 × 12 mm gaussian filter. The voxel count was normalized to the cerebellar ROI value. Images of the MCI-NC, MCI-C and AD groups, including patients with AD1 and AD2, were compared with those of the aged normal controls by means of a between-group analysis ($p < 0.05$ with false discovery rate correction; extent threshold: $k = 750$). For group analysis, a two-sample t test was used to detect differences among the groups.

In addition, a Z-score map of individual PET images was created for comparison between the mean and SD of the PET images of aged normal controls for each voxel. A software program named the Easy Z-Score Imaging System was used for this analysis [18]. Each PET SUV image was compared with the mean and SD of PET images of 15 aged normal controls (age: 58.9 ± 13.5 years; gender M/F: 10/5; MMSE score: 29.9 ± 0.2), using voxel-by-voxel Z-score analysis following voxel normalization to cerebellar ROI values according to the following formula: Z-score = (control mean – individual value)/control SD. Z-score maps were displayed by projection, with an averaged Z-score of 14 mm thickness to the surface rendering the anatomically standardized MRI template.

Neuropathological Staining

Postmortem brain tissue from an autopsy-confirmed AD case (87-year-old male) was obtained from the Tohoku University Hospital. Serial sections (6 μm thick) of paraffin-embedded blocks of temporal and frontal cortices were prepared in xylene and ethanol. Before staining, quenching of autofluorescence was performed by blanched sections in 0.25% potassium permanganate solution for 30 min. The sections were then treated with 0.1% potassium metabisulfite and 0.1% oxalic acid, followed by dipping briefly in water. The quenched tissue sections were immersed in 100 μmol/l of compound solution for 10 min and examined using a BX-51 fluorescence microscope (Olympus, Tokyo, Japan) equipped with a violet filter set (excitation: 380–420 nm; dichroic mirror: 430 nm; long-pass filter: 450 nm). Immunostaining was performed using monoclonal antibodies against Aβ (6F/3D; Dako, Glostrup, Denmark) at a dilution of 1:50. After pretreatment with formic acid for 5 min, the sections were placed in blocking solution for 30 min. After incubation with primary antibodies at 37°C for 60 min, the sections were processed by the avidin-biotin method using the Pathostain ABC-POD(M) kit (Wako) and chromogen DAB. The amyloid plaque morphology was classified into 2 types: (1) dense Aβ plaques including cored deposits with or without a ring of neuritic fibers, and (2) diffuse Aβ plaques including amorphous deposits. We randomly selected 20 areas (1.05 mm^2 per area) per section in the gray matter of the frontal and temporal cortices and counted the number of dense and diffuse Aβ plaques in each area. To estimate the capability of the compound to detect each kind of plaque, we examined the relationship between the number per unit area of positive staining using BF-227- and Aβ-specific antibody.

Statistical Analysis

Statistical comparisons of age among the 5 groups were performed using the Kruskal-Wallis test followed by Dunn's multiple comparison test. Statistical comparison of ROI results was performed via an analysis of variance followed by the Bonferroni method for multiple comparisons. Furthermore, effect size coefficients (Cohen's d) were calculated to evaluate group differences in PET measurements. The performance of diagnostic indices to

discriminate among groups was assessed using receiver operating characteristic (ROC) analysis. The area under the ROC curve (AUC) and SE were calculated and compared using GraphPad Prism software (GraphPad, San Diego, Calif., USA). Correlations between stainability of Aβ immunostaining and BF-227 staining were examined using the nonparametric Spearman rank correlation analysis. The paired t test was used to examine the difference in cored plaque density between the frontal and temporal cortices. Statistical significance for each analysis was defined as $p < 0.05$. These analyses were performed using GraphPad Prism software.

Results

A statistically significant difference in age between aged normal controls and patients with MCI ($p < 0.05$) was observed. However, no statistically significant difference in age between MCI-C and MCI-NC as well as between aged normal controls and patients with AD was observed. Patients with AD showed a significantly lower MMSE score than aged normal controls. In addition, the AD2 group showed a significantly lower MMSE score than the MCI-NC group. However, no statistically significant difference in MMSE score was observed among other groups.

Voxel-based analysis of [^{11}C]BF-227 PET images demonstrated that MCI-C and patients with AD had significantly higher [^{11}C]BF-227 uptake in the neocortical region than aged normal controls (fig. 1; tables 2, 3). Bilateral temporoparietal BF-227 uptake was evident in both the AD and MCI-C groups although significant uptake in the posterior cingulate cortex and precuneus was observed only in the AD group. In the AD and MCI-C groups, the difference in the lateral frontal cortex was less evident compared with that in the lateral temporoparietal region. In contrast to the MCI-C group, the MCI-NC group showed no significant elevation of BF-227 uptake compared with the aged normal control group. Z-score maps of PET images were created by comparison with the normal control database (fig. 2). Most patients with AD showed a Z-score greater than 2 in the bilateral temporal and posterior cingulate cortices. In contrast, 10 out of the 12 aged normal controls (83%) showed no remarkable change in neocortical BF-227 uptake, except for 2 subjects (17%) showing modest changes in the lateral temporal and cingulate cortices. MCI-C tended to show higher neocortical Z-scores than MCI-NC (fig. 2b). Among the 7 MCI-C, 4 showed BF-227 uptake in the bilateral temporoparietal and frontal cortices, while the other 2 showed moderate abnormality in the temporal and frontal Z-scores. In MCI-C, changes in BF-227 uptake within the posterior cingulate cortex were relatively moderate compared with those in the lateral temporal cortex. One MCI-C showed limited change in BF-227 uptake within the temporal cortex and precuneus. In contrast to MCI-C, most MCI-NC showed no abnormal BF-227 uptake in the lateral temporal cortex, except for 1 who showed a slightly higher Z-score in the temporal cortex and an extremely high score in the posterior cingulate cortex. Another 3 MCI-NC also showed limited abnormality in the posterior cingulate cortex and precuneus but no abnormal Z-score in the lateral temporal cortex. No significant difference in BF-227 uptake was observed between the MCI-NC and MCI-C groups, MCI-NC and AD groups, and MCI-C and AD groups. Furthermore, no significant region showing reduction in BF-227 uptake in the MCI and AD groups compared with the aged normal controls was observed.

ROI analysis data were roughly consistent with voxel-based analysis data (fig. 3; table 4). The MCI-C group showed higher retention of [^{11}C]BF-227 in the frontal, temporal and parietal cortices than the aged normal control group. The AD1 group showed higher BF-227 retention in the frontal, temporal, parietal and occipital cortices than the aged normal control group. The AD2 group showed higher BF-227 retention in the temporal, parietal, occipital and posterior cingulate cortices than the aged normal control group, with the exception of the frontal cortex. Furthermore, significantly higher BF-227 uptake

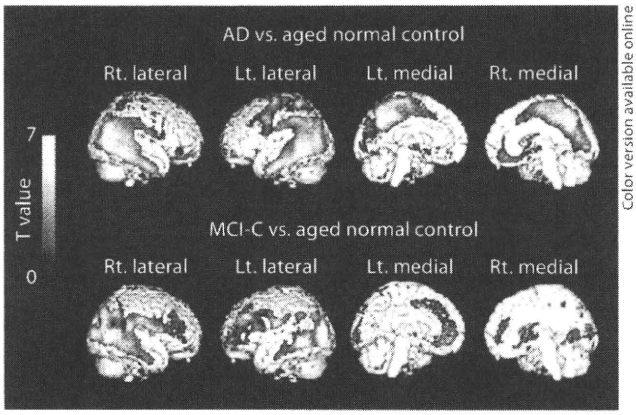

Fig. 1. Brain regions showing significantly higher uptake of [^{11}C] BF-227 in patients with AD (upper images) and MCI-C (lower images) compared with data from aged normal controls ($p < 0.05$, corrected for multiple comparisons). The red-to-yellow scale indicates the level of statistical significance of the differences in [^{11}C]BF-227 uptake (yellow: most significant difference).

Table 2. Talairach coordinates of within-cluster peak areas showing significantly higher BF-227 uptake in AD patients compared with aged normal group ($p < 0.05$, false discovery rate corrected)

k	T value	Talairach coordinates			Region
		x	y	z	
48,058	7.15 (5.38)	54	−46	−12	right inferior temporal gyrus
	6.79 (5.21)	50	−62	14	right middle temporal gyrus
	6.22 (4.92)	−52	−58	−2	left middle temporal gyrus
760	4.81 (4.09)	−24	4	−4	left putamen

Values in parentheses denote Z values.

Table 3. Talairach coordinates of within-cluster peak areas showing significantly higher BF-227 uptake in MCI-C compared with aged normal group ($p < 0.05$, false discovery rate corrected)

k	T value	Talairach coordinates			Region
		x	y	z	
14,893	6.19 (4.42)	46	−64	6	right middle temporal gyrus
	5.84 (4.27)	40	−74	14	right middle temporal gyrus
	5.52 (4.12)	52	−44	−8	right temporal lobe subgyrus
6,768	5.78 (4.24)	−36	32	34	left middle frontal gyrus
	4.78 (3.75)	−58	−16	24	left parietal lobe
	4.70 (3.71)	−24	50	0	left superior frontal gyrus
5,893	5.77 (4.24)	−38	−80	10	left middle occipital gyrus
	5.52 (4.12)	−42	−60	−4	left middle temporal gyrus
	5.27 (4.00)	−22	−92	−4	left cuneus

Values in parentheses denote Z values.

was found in the frontal and temporal cortices of the MCI-C group as well as in the temporal and parietal cortices of the AD group compared with the MCI-NC group. Compared with the AD group, Cohen's d was higher in the temporal (2.93) and parietal (2.25) cortices than in the frontal (1.69) and posterior cingulate (1.51) cortices for the aged normal control group. When comparing the MCI-C and MCI-NC groups, the highest Cohen's d was observed in the temporal (1.70) and parietal (1.76) cortices, followed by the frontal (1.62), posterior cingulate (0.85) and occipital (0.37) cortices, indicating that the difference in SUVR is the largest in the temporoparietal cortex when comparing the MCI-C and MCI-NC groups. Furthermore, ROC analysis demonstrated higher AUC values with the temporal SUVR (AUC = 0.987; SE = 0.016) than with the frontal SUVR (AUC = 0.915; SE = 0.052) for the discrimination between the AD and aged normal control groups as well as between the MCI-C and MCI-NC groups (fig. 4). Using the temporal BF-227 SUVR of 1.10 (1.5 SD above control mean) as the cutoff, a sensitivity of 95% and specificity of 92% in the discrimination between AD and aged normal groups, and a sensitivity of 100% and specificity of 57% in the discrimination between MCI-C and MCI-NC was achieved.

To explain why BF-227 preferentially accumulates in the temporal cortex as opposed to the frontal cortex of the AD brain, we examined the binding characteristics of BF-227 to Aβ deposits, using postmortem AD brain samples. BF-227 showed good stainability for dense-type plaques in the frontal and temporal cortices. Diffuse plaques in the frontal cortex tended to be larger than those in the temporal cortex. However, the stainability for diffuse-type plaques in the frontal cortex was relatively weaker than that in the temporal cortex (fig. 5). The mean number of Aβ plaques positively stained with BF-227 was significantly higher in the temporal cortex than in the fron-